International Journal of Technology (2018) 1: 5-15
ISSN 2086-9614

AN INTEGRATED SYSTEM FOR ENHANCING FLEXURAL MEMBERS' CAPACITY VIA COMBINATIONS OF THE FIBER REINFORCED PLASTIC USE, RETROFITTING, AND SURFACE TREATMENT TECHNIQUES

Sri Tudjono[1], Han Ay Lie[1], Buntara Sthently Gan[2*]

[1]*Department of Civil Engineering, Faculty of Engineering, Diponegoro University, Tembalang, Semarang 50275, Indonesia*
[2]*Department of Architecture, College of Engineering, Nihon University, Koriyama, Fukushima 963-8642 Japan*

(Received: May 2017 / Revised: December 2017 / Accepted: January 2018)

ABSTRACT

This paper elaborates on the theoretical background, necessity, and techniques for enhancing the flexural capacity of a T-section member under combined bending and shear. The paper is based on a continuing research program seeking solutions to the design disparities arising from the introduction of new seismic codes and revised earthquake mapping prior to the tsunami and major earthquakes that occurred in South East Asia more than a decade ago. The research considered the application of external reinforcement using fiber-reinforced polymer (FRP) sheets, creating confinement in the shear area, and improving the tensile strength zone. The test results suggested that the methods sufficiently increased the load-carrying capacity to meet the new provisions, but they also showed that the optimum load-carrying capacity was not reached due to debonding of the FRP sheets in the tensile zone. The work was expanded to search for a surface treatment method that could shift the failure mode from debonding to FRP rupture by performing direct shear tests on treated FRP-to-concrete bond surfaces. Using the best surface treatment method, a failed member was straightened, retrofitted, and re-reinforced in terms of both shear and tension. The experimental results showed that the load-carrying capacity of the flexural member not only increased significantly, but the surface treatment methods also overcame the interface debonding problem. This research provides a method for upgrading the flexural capacity of T-section members designed prior to the tsunami and earthquakes of 2004, and it offers a solution for cracked section repair and restoration.

Keywords: FRP reinforcement; Retrofitting; Surface treatment

1. INTRODUCTION

The tsunami that occurred in South East Asia in 2004, which was followed by a series of earthquakes, drastically changed the approach to structural design. The major revision in the earthquake mapping in the region affects the spectrum response and storey-drift criteria, resulting in much higher load-carrying capacity requirements for concrete elements. Under severe horizontal loading, a rigid frame is subjected to high shear stresses in combination with large bending moments. The ACI 440.2R provision includes separate guidelines for external fiber-reinforced polymer (FRP) flexure and shear reinforcement. However, a combination of external FRP sheets customized for shear and flexure substantially improves the bending

*Corresponding author's email: buntara@arch.ce.nihon-u.ac.jp, Tel: +81-90-2483-1161, Fax: +81-90-2483-1161
Permalink/DOI: https://doi.org/10.14716/ijtech.v9i1.298

capacity of a member (Spadea et al., 2015; Tudjono et al., 2015).

FRP reinforcement is situated in the tensile area, enhancing the section's performance, since the concrete is weak in tension. A structure's beam section is subjected to a combination of shear and bending moment stresses produced by gravity (Figure 1a) and seismic loads (Figure 1b).

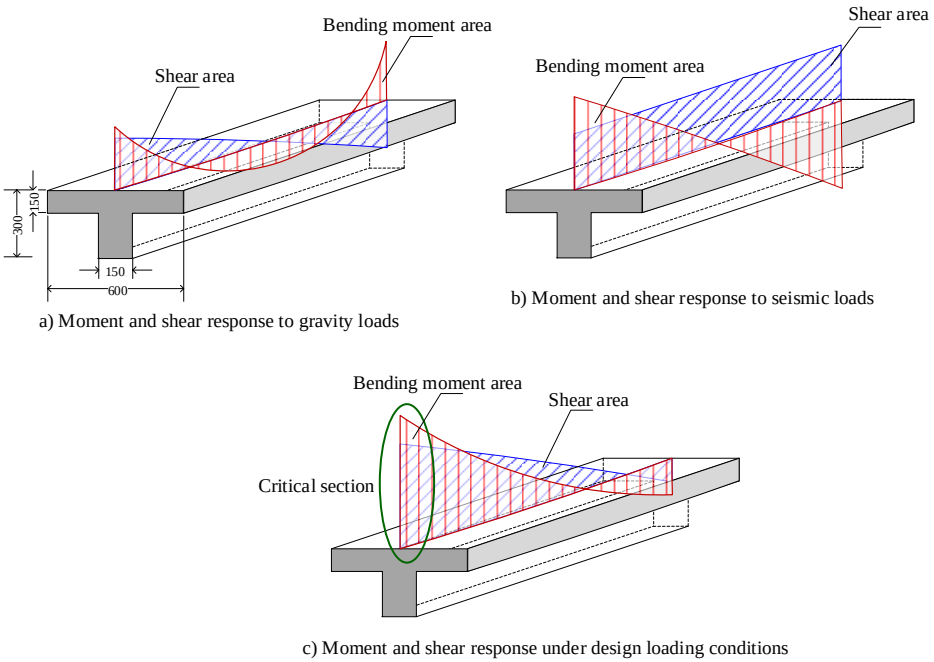

Figure 1 Bending moment and shear stresses under combined loading

Under combined loading (Figure 1c), the beam-to-column area of the beam is the section that will experience the largest bending moment in combination with high shear stresses. The member undergoes a negative bending moment, and part of the floor slab could function as the flanges of a T-section. Since the flanges are in tension, the FRP tensile reinforcement is attached to this area. The presence of columns and walls or partitions limits the overall placement of sheets over the entire flange; thus, the FRP is situated to the left and right of the flange (Figure 2). This method was chosen to simulate the actual behavior of a beam in a structure. A U-shaped shear reinforcement is applied along the web of the beam (Figure 2b).

The aim of this study was to propose a solution for enhancing the flexural members' capacity via external FRP reinforcement. The FRP reinforced specimens were designated as BFRP. The developed system was also used in combination with retrofitting techniques for failed members. Optimization was conducted by improving the bond area between the FRP and concrete to prevent debonding. When applying external FRP reinforcements, a crucial factor is that the composite action between the FRP and concrete should be maintained until the member fails. A study on the bond behavior of FRP sheets revealed that the bond depends on the preparation of the contact surface, geometry of the FRP sheet, strength of the concrete, and characteristics of the bonding agent (Tudjono et al., 2017). This research work was conducted in three phases, as described below.

The first phase of this study was the evaluation of the capacity enhancement due to external tensile and shear FRP reinforcements (Tudjono et al., 2015). The load-deformation responses were recorded and compared with an identical section with no FRP reinforcements. This controlling element (BC) was designed based on the previous standards. The work focused on the issue of whether the proposed method could upgrade the structural elements to meet the new

provision. Since ductility also plays a major role in the earthquake code, the moment-rotation performance of the beam under a monotonic load increment was also monitored and analyzed.

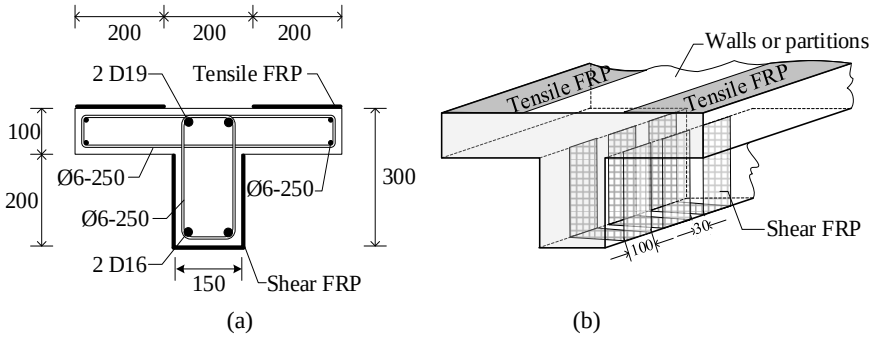

Figure 2 Placement of Fiber Reinforced Plastic (FRP) sheets for tensile and shear reinforcement: (a) tensile reinforcement; (b) shear reinforcement

The test results on the BFRP specimens were satisfactory in terms of flexural capacity enhancement. However, debonding between the FRP and the concrete surface was observed, suggesting that the improvement could be optimized by enhancing the bond performance.

The second phase was to seek a concrete surface preparation that could improve the FRP-to-concrete bond performance (Tudjono et al., 2017). Variations in the surface preparations were established by applying grooves on the concrete surface, and the preparations were tested under shear and direct tension. The results showed that a preparation with 3-mm grinding and sand blasting, as advised by the manufacturer, was not sufficient for ensuring the bond between the FRP and concrete. The surface preparation with the application of grooves was further adopted for the next phase.

In the third phase, a failed, cracked element was straightened and retrofitted. The retrofitted beam element (BR) was reinforced using FRP sheets in the same manner as the BFRP from the first phase. The newly introduced surface preparation from the second phase was applied prior to the FRP attachment. This combined method provided insight into the optimization of FRP reinforcement, as well as suggesting a revitalization method for failed members.

2. FRP REINFORCEMENTS AND RETROFITTING

2.1. FRP Reinforcements

The FRP sheets used in this study consists of woven, unidirectional carbon fibers (Figure 3a). The sheets were designed for dry application, consisting of 99% black carbon fibers by weight as the warp, with 1% white thermoplastic heat-set fibers as the weft. The sheet thickness measured 0.131 mm for a single sheet. The individual fibers had a tensile modulus of 234 GPa, with a tensile strength of 3.5 MPa. The maximum strain was measured to be 0.018. When attached to the concrete, the bonding agent and the FRP fibers will emerge as a unity. The test reports on the integrated material were based on the single lap shear test and conducted at the Laboratoire Mécanique Matériaux et Structures in Lyon (Gicquel et al., 2006).

The bond properties of the interlaminar material are shown in Figure 3b. The interface exhibited a linear behavior up to failure with a shear strength of 16.6 MPa. The maximum elongation over a bond length of 25 mm was 0.009 mm, which is much higher than the ultimate concrete tensile strain. The test results of the bond behavior suggested a good compatibility between the interlaminar material and concrete in the shear area. In addition, for low strains, the concrete response was linear, and disparities in stress-strain characteristics did not influence the behavior.

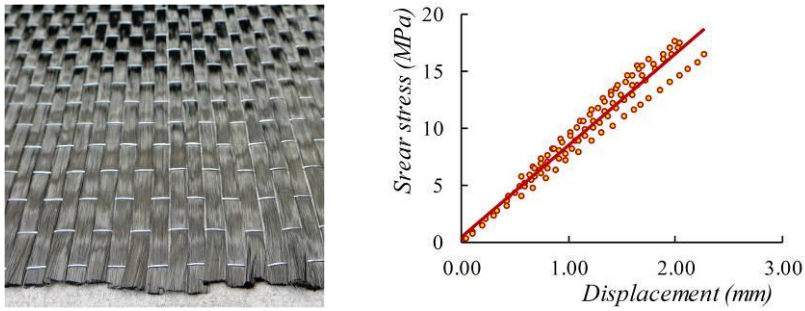

(a) (b)

Figure 3 Shear properties of the FRP and bonding agent (Gicquel at al., 2006): (a) FRP sheet; (b) FRP bond shear

The test specimens in this study had a cylindrical compressive strength of 37.4 MPa, resulting in a theoretical shear strength of 6.1 MPa, in accordance to the *fib* model code 2010. The FRP sheets were applied to the concrete surface using a two-component, carbon-epoxy agent produced using the *pultusion* method (a manufacturing method for composite materials employing the pulling technique). For both tension and shear reinforcement, a single ply was used. The concrete surface was prepared in accordance with the test results from the second phase (Figure 4a and 4b). A thin layer of bonding agent was applied (Figure 4c), followed by FRP wrap placement (Figure 4d).

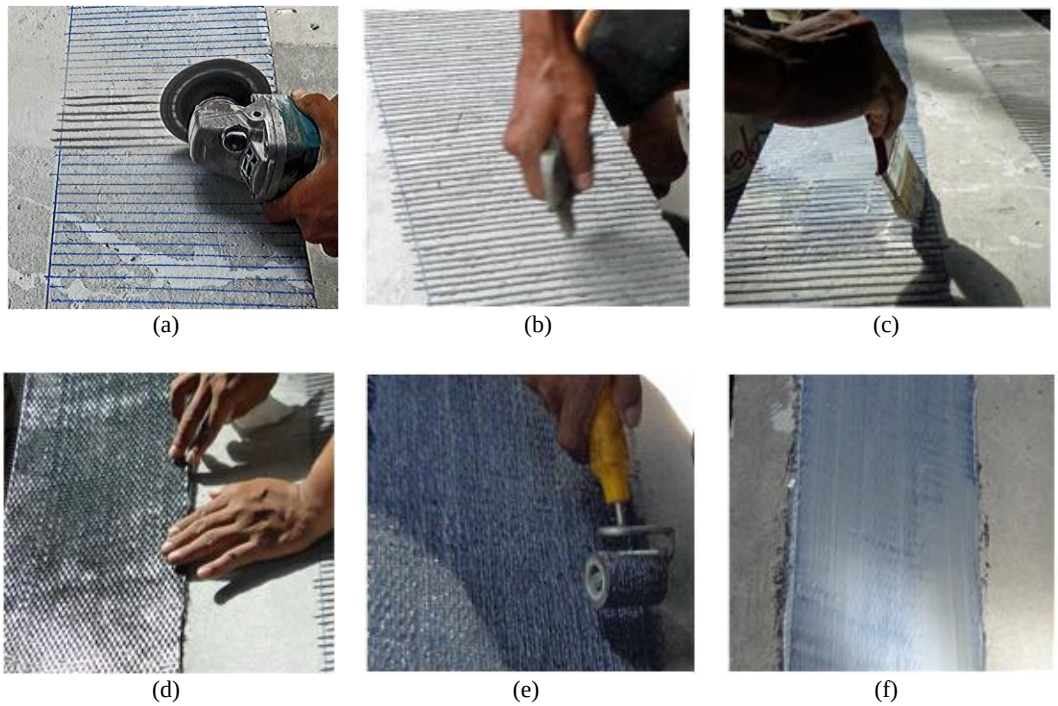

(a) (b) (c)

(d) (e) (f)

Figure 4 FRP application: (a) surface preparation; (b) sand blasting; (c) first epoxy layer; (d) FRP application; (e) attaching treatment; (f) final epoxy layer

Pressure was applied to the FRP using a roller to ensure a good bond between the concrete and FRP sheets (Figure 4e). A second layer of bonding agent was put on top of the FRP sheet, and the reinforcement was cured for a week, thereby allowing the bonding agent to develop its fullest adhesive capacity (Figure 4f).

2.2. FRP Shear Reinforcement

There are several types of shear reinforcement, including U-jacketing, strips bonded to the sides only, and complete wrapping of the sections. This research used a partial U-jacketing system, ending at the intersection between the flanges and web of the T-section. The study by Cao et al. (2005) suggested that the FRP rupture mode is governed by complete wrapping and U-jacketing, while strips resulted in a failure mode characterized by debonding. Based on these findings, the test specimen was designed so that the beam failed in flexure. The FRP shear reinforcement was situated along the entire beam, providing additional confinement in the section's compression zone. The benefit of confinement was clarified by Antonius (2015) and Boonpichetvong et al. (2016), who demonstrated that the concrete strength was positively influenced by the hoop confinement.

The confining stress influences the compressive strength enhancement, and it is a direct function of the lateral strain (Kwan et al., 2015). According to the fib-CEB 2010, the compressive strength increase due to the confining effect is approximately 20%. To guaranty composite continuity, the distance between the shear sheets was determined based on the ACI 440.2R code.

2.3. FRP Flexure Reinforcement

The FRP reinforcement has two major functions. First, it causes the flexure element's strengthening in meeting the new provisions for seismic performance, and second, it repairs and restores the load-carrying capacity of cracked elements. The latter is achieved by a combination of FRP reinforcement and retrofitting. When tensile reinforcements reach their yield, the tensile stresses are transferred to the FRP. There are two theoretical modes of failure, as follows: failure in the FRP and concrete crushing in the compression area. Failure in the FRP is categorized as bonding failure under shear forces or rupture of FRP sheets in tension. The shear reinforcements provide resistance to shear stresses, while enhancing the concrete compressive strength due to the confining effect.

2.4. Surface Treatments

The failure modes of the interface in the FRP-to-concrete bond are an integrated function of several factors, namely the strength and area of the FRP-to-concrete bond in tension, the number of FRP sheets and their strength, and the concrete shear capacity. During the first phase of this research work, the failure was governed by debonding. To shift the failure mode and increase the beam's capacity, a series of tests on the proposed surface treatments were conducted (Tudjono et al., 2017). The research concluded that the surface treatment advised by the FRP producer, involving a 3-mm grinding and sandblasting, is satisfactory for a direct tension response, but results in 75% debonding under shear conditions.

The surface was treated by applying a variation in the configuration of 2×0.5 mm grooves, which were made 10 mm apart. The research results showed that a groove configuration perpendicular to the shear direction is satisfactory in preventing debonding. The test results also underlined Teng et al.'s (2002) finding that high stress concentrations are present at the edges of the FRP.

3. TEST PROGRAM

The configuration and test setup for the first and third phases are shown in Figure 5. To induce a negative moment in combination with a maximum shear force, the T-sections were placed top down and subjected to a one-point loading system (Figure 6). This configuration ensured a simultaneous maximum bending and shear stress at the midspan. The beam was simply supported and under-reinforced with a reinforcement ratio (ρ) of 0.013. This type of configuration is customarily used in research (Ceroni, 2010; Ceroni et al., 2016; Huang et al.,

2016).

The beams were loaded with a 120 N/sec monotonic load increment. The load and deformation responses were recorded using a load cell and Linear Vertical Displacement Transducers (LVDTs). Material responses, FRP (type BFLA 5) and steel reinforcement (type FLA 6-11), and concrete in compression and tension (type PFL 60-11-1L) were monitored using strain gauges. To ensure a straight alignment during loading, two horizontal LVDTs were placed on both sides to monitor the beam's lateral response. Additional strain gauges were placed on the FRP shear sheets.

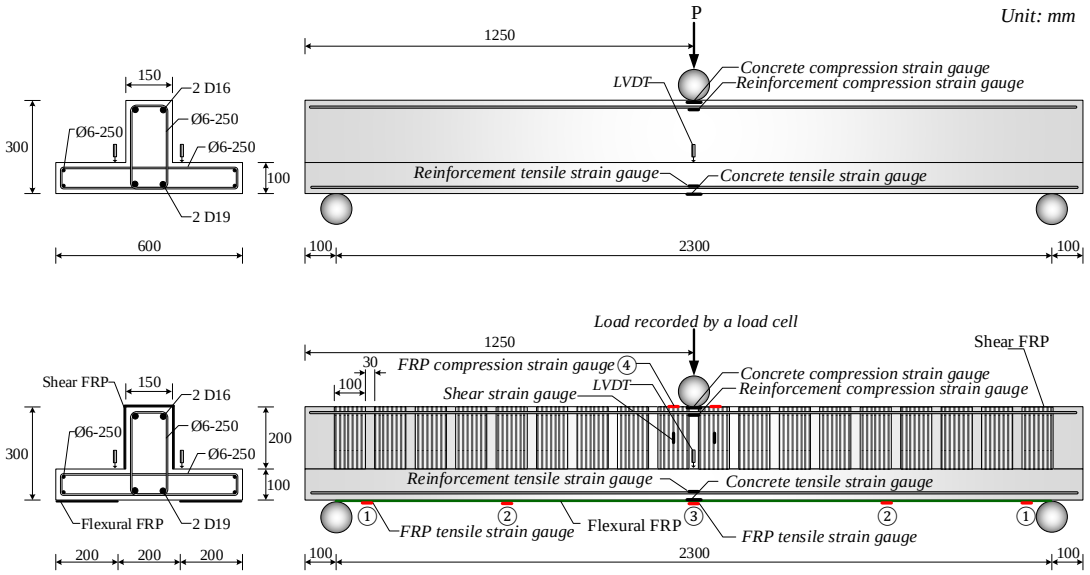

Figure 5 Test setup

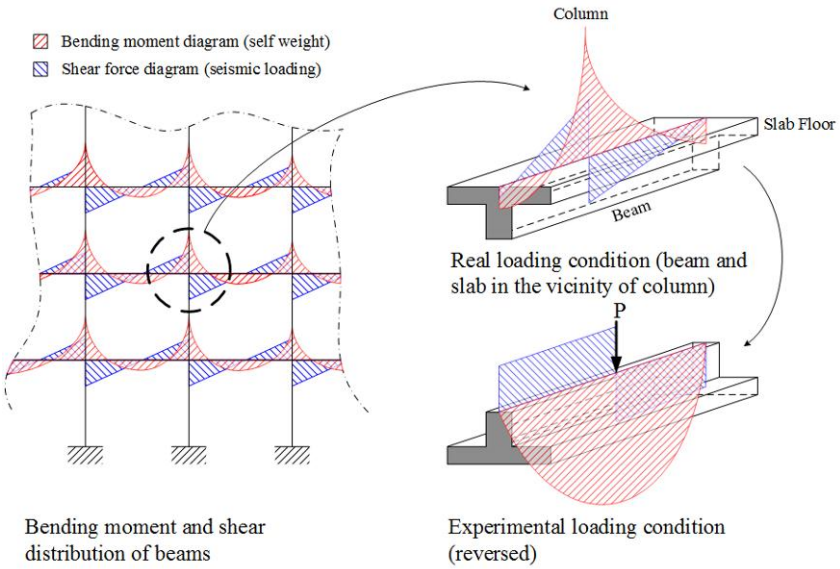

Figure 6 Testing mechanism and stress responses

Three beam types were tested, as follows: the controlling element, BC; the FRP-reinforced beam, BFRP; and the retrofitted and FRP-reinforced beam, BR (Tudjono et al., 2015; Tudjono et al., 2017). For every category, two specimens were prepared. In addition, 100×200 mm cylinders were generated to provide the 28th day concrete strength. The steel reinforcement had a yield stress (f_y) of 405 MPa.

3.1. Reinforced Beam Failure in Debonding

The first phase of the experimental research resulted in debonding between the FRP and the concrete in tension-shear stress due to differentiations in the shear stresses in this interface. This behavior was strengthened by the direct shear performance tests in the second phase (Tudjono et al., 2017). Initial cracks in the transversal direction were observed in the concrete area between the FRP reinforcements. The cracks propagated to the flanges of the beam. These findings supported the study conducted by Leung (2006), who stated that debonding emerges at the bottom of a flexure crack and propagates toward the sheet's end. Debonding occurs due to the fracture of a thin layer of concrete. Coronado and Lopez (2005) explained that the bond failure mechanism is initiated by the formation of concrete microcracks close to the interface. On further loading, these cracks form bridges, transforming into macrocracks, and this leads to the debonding mechanism. The loading was terminated due to bond failure.

The FRP-reinforced beams had a load increase of 37% at the initial cracking stages, and an enhancement of 26% at yielding. This improvement mainly originated from the additional tensile force provided by the FRP sheets and the concrete strength enhancement due to confinement in the compression zone.

3.2. Retrofitting and Bond Optimization

The controlling beams, BC, were straightened by applying a reverse load. The alignment was carefully monitored, ensuring a perfectly flat specimen. The cracks were retrofitted using an epoxy resin solution (Tudjono et al., 2017) and reinforced with FRP sheets identical to the BFRP specimens. These specimens were denoted BR. The BR specimens were tested in the exact same manner as conducted for BC and BFRP. Since the reinforcing steel yielded during the first stage of this experiment, no distinguishing yield point was detected. The load-displacement response followed a nonlinear path up to failure, followed by a sudden collapse distinguished by the rupture of the FRP in tension (Figure 7a). The cracks in the concrete propagated vertically toward the neutral axis (Figure 7b).

(a) (b)

Figure 7 Failure mode of the BR specimens in FRP rupture: (a) FRP rupture; (b) beam collapse

4. RESULTS AND DISCUSSION

The controlling element BC was characterized by an under-reinforced failure mode. The concrete cracked in the tensile area, and the tensile reinforcements yielded. The cracks in the tensile area of the beam propagated toward the neutral axis, followed by crushing of the concrete in the compression area. The BFRP underwent cracking in the un-FRP-reinforced strip of the concrete in tension, the steel reinforcement yielded, and the bond between the FRP and concrete failed under shear tension. The retrofitted FRP-reinforced beam, BR, followed the same pattern as BFRP, but since a better bond was achieved in the interface, the loading could be increased. The failure of the member was due to a rupture in the tensile FRP. The ultimate load data at various stages for BC, BFRP, and BR are presented in Table 1.

Table 1 Loads at initial cracking, steel yielding, FRP debonding, and FRP rupture

Specimen	Load (kN) and load ratio to BC			
	Initial cracking	*Reinforcement yielding*	*Debonding*	*FRP rupture*
BC	25.3 (1.00)	85.0 (1.00)	-	-
BFRP	34.8 (1.38)	107.0 (1.26)	126.7 (1.49)	-
BR	34.7 (1.37)	-	-	169.2 (1.99)

4.1. Load Displacement

The load-displacement behavior of externally reinforced beams is influenced by the material's mechanical properties and the FRP configurations (Attari et al., 2012). The load and vertical displacement at the midpoint for all three beam types are shown in Figure 8. The BC controlling beams demonstrated a clear yielding point, followed by a near-horizontal yielding plateau. The yielding was confirmed by the data obtained from the steel strain gauges, showing that the steel strain reached 2.05×10^{-3} at failure. At further loading stages, extensive crack propagations toward the neutral axis of the beam were observed. The concrete in compression near the load was crushed, as underlined by the concrete strains, which exceeded 3×10^{-3}.

The BFRP reinforced beam had a substantially higher load-carrying capacity, with an increase of 49% over the controlling element; 27% of this was the contribution of the tensile FRP, while 22% corresponded to the increase in the confined compressive strength. A faint yielding plateau was seen, and the failure was due to FRP debonding under shear stress. The debonding behavior was unmistakably nonlinear and had a softening branch due to the shear slip behavior (Freddi & Savoia, 2007).

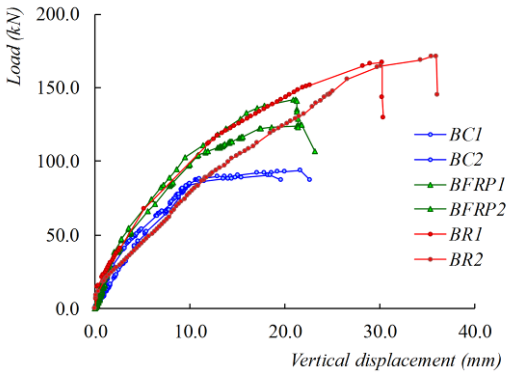

Figure 8 Load-displacement responses

The BR retrofitted specimens did not exhibit yielding, and for analytical purposes, the yield point was determined using the 0.2% offset method. The initial cracking occurred at load levels comparable to those of the BFRP specimens. Visual observation revealed that the cracks initiated in the uncracked concrete rather than the retrofitted areas, suggesting that the retrofitting resulted in a stronger material compared with the concrete. Improving the interface performance between the FRP and concrete contributed a 99% capacity improvement to BC, and no post-peak curve was detected for the BR elements.

4.2 Strain Behavior

The responses of the FRP in tension were monitored by strain gauges situated close to the supports ①, at one-fourth ②, and at mid-span ③ (Figure 9a). The strain behaviors of both the BFRP and BR elements were similar, and it is clear in the bending moment diagram that the strain in the FRP followed the deformation intensity. The behavior of gauges ② and ③ were nonlinear, influenced by the responses of the concrete. Near the support at gauge ①, the strain

behavior was dominated by the linear characteristics of the FRP, and it was almost linear up to failure. The restriction of concrete in compression is a function of strain in the shear FRP, and this was reflected by the load-strain response of strain gauge ④, as shown in Figure 9b.

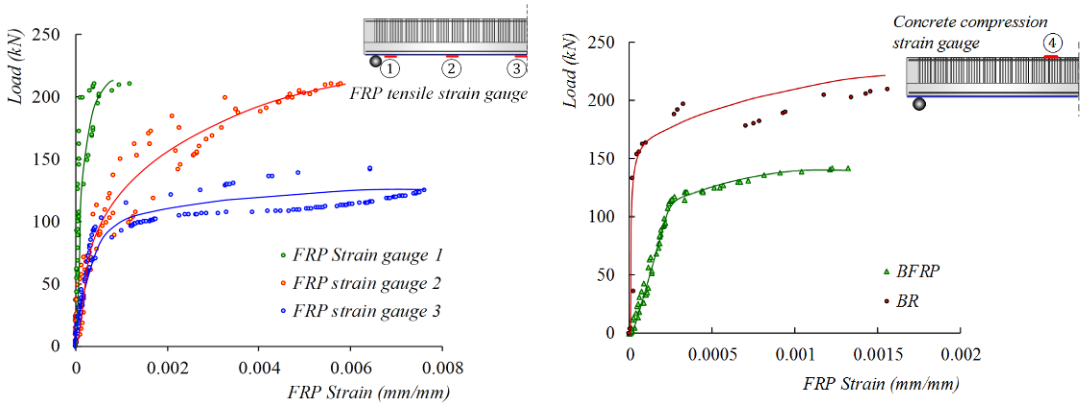

Figure 9 Tensile FRP strain response: (a) tensile FRP response; (b) compression FRP response

4.3. Flexural Capacity and Confinement

The confinement effect was studied through the strain behavior of the FRP in compressions. The load-strain responses of BFRP and BR were similar, but the retrofitted member had a much lower strain rate compared with the BFRP member. The following factors were considered: the modulus of elasticity of steel E_s remains constant during all loading stages; the increase in compressive strength due to confinement does not significantly alter the concrete's modulus of elasticity E_c; and the volumetric ratio of the epoxy is small compared with that of the concrete.

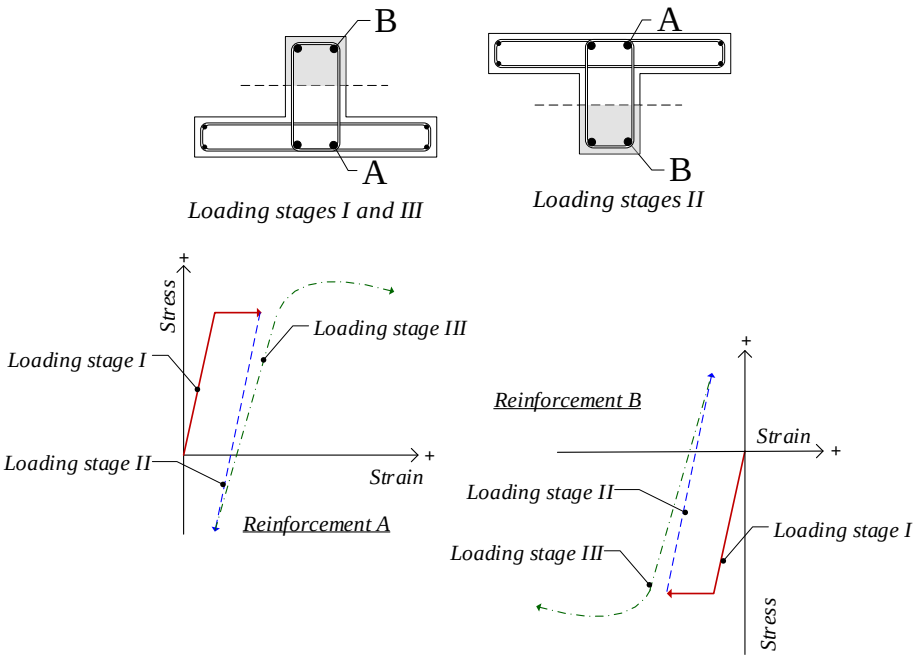

Figure 10 Prestress mechanism in the section due to retrofitting

The increase in capacity of the retrofitted element can be explained as follows: During the testing sequence, the steel reinforcement of the retrofitted beam BR underwent three stages. In stage I, reinforcements A were subjected to tensile strains, while reinforcements B underwent linear compression. The strain gauge data provided information that both the steel bars A and B

had yielded. In stage II, the beam was straightened, resulting in a reverse strain for both reinforcements A and B. The load was maintained until the injected epoxy-resin hardened, creating a precompression condition for the steel bars. The retrofitting also restored the bond between the steel reinforcements and concrete. Thus, when entering loading stage III, the flange area of concrete and the steel A were in precompression, while reinforcing steel B was in pretension (Figure 10).

Upon loading, the prestressing strains created an additional load-carrying capacity for the steel bars. The confinement provided by the U-jacketing FRP sheets in combination with the prestressing of concrete and steel resulted in a higher moment of inertia of the section; thus, under the same loading, the BFRP member yielded in a relatively stiffer member.

5. CONCLUSION

This research considered the behavior of a T-section subjected to bending moments in amalgamation with maximum shear stresses, as would be the case in structures subjected to gravity and seismic loadings. The method provided sufficient improvement for typical sections to meet the newly introduced earthquake standards. The increase in the load-carrying capacity was mainly due to the additional tensile reinforcements provided by the FRP and the concrete compressive strength confinement from the external shear reinforcement. This external shear reinforcement led to a higher cylindrical compressive strength in the compression areas of the section. The shear reinforcement granted sufficient strength to carry the high shear stresses in the web of the section. The proposed surface preparation method by applying 2×0.5 mm grooves, 10 mm apart and perpendicular to the tension direction, was sufficient to prevent debonding under tensile-shear stress.

An approach to simultaneously optimizing the flexural capacity and performing retrofitting and FRP reinforcement was proposed. The revitalized members performed excellently in terms of both bending and shear. The members' load-carrying capacity increased 99% in comparison with the controlling element BC.

6. REFERENCES

ACI 440.2R-08, 2008. *Guide for the Design and Construction of Externally Bonded FRP Systems for Strengthening Concrete Structures*. American Concrete Institute, USA

Antonius, 2015. Strength and Energy Absorption of High-strength Steel Fiber-concrete Confined by Circular Hoops. *International Journal of Technology*, Volume 2(2), pp. 217–226

Attari, N., Amziane, S., Chemrouk, M., 2012. Flexural Strengthening of Concrete Beams using CFRP, GFRP and Hybrid FRP Sheets. *Construction and Building Materials*, Volume 37, pp. 746–757

Boonpichetvong, M., Pannachet, T., Pinitkarnwatkul, S., 2016. Finite Element Modelling Confined with Metal Sheet Strips. *International Journal of Technology*, Volume 7(7), pp. 1132–1140

Cao, S.Y., Chen, J.F., Teng, J.G., Hao, Z., Chen, J., 2005. Debonding in RC Beams Shear Strengthened with Complete FRP Wraps. *Journal of Composites for Construction*, Volume 9(5), pp. 417–428

Ceroni, F., 2010. Experimental Performances of RC Beams Strengthened with FRP Materials. *Construction and Building Materials*, Volume 24(9), pp. 1547–1559

Ceroni, F., Ianniciello M., Pecce M., 2016. Bond Behavior of FRP Carbon Plates Externally Bonded Over Steel and Concrete Elements: Experimental Outcomes and Numerical Investigations. *Composites, Part B*, Volume 43(2), pp. 99–109

Coronado, C.A., Lopez, M.M., 2005. Sensitivity Analysis of Reinforced Concrete Beams Strengthened with FRP Laminates. *Cement & Concrete Composites*, Volume 28, pp. 102–114

fib-CEB Model Code for Concrete Structures 2010, 2013. Fédération International du Béton, Lausanne, Switzerland

Freddi, F., Savoia, M., 2007. Analysis of FRP–concrete Debonding via Boundary Integral Equations. *Engineering Fracture Mechanics*, Volume 75, pp. 1666–1683

Gicquel, Y., Hamelin, P., Ferrier, E., 2006. *Test report Laboratoire Mécanique Matériaux et Structures*. No. SIKA/06/01 du 04/05/06, Université de Lyon I, France

Huang, L., Yan, B., Yan, L., Xu, Q., Haozhi, Kasal, B., 2016. Reinforced Concrete Beams Strengthened with Externally Bonded Natural Flax FRP Plates. *Composites, Part B*, Volume 91, pp. 569–578

Kwan, K.H., Dong, C.X., Ho, J.C.M., 2015. Axial and Lateral Stress–Strain Model for FRP Confined Concrete. *Engineering Structures*, Volume 99, pp. 285–295

Leung, C.K.Y., 2006. FRP Debonding from a Concrete Substrate: Some Recent Findings Against Conventional Belief. *Cement & Concrete Composites*, Volume 28, pp. 742–748

Spadea, G., Bencardino, F., Sorrenti, F., Swamy, R.N., 2015. Structural Effectiveness of FRP Materials in Strengthening RC Beams. *Engineering Structures*, Volume 99(15), pp. 631–641

Teng, J.G., Chen, J.F., Smith, S.T., Lam, L., 2002. *FRP Strengthened RC Structures*. John Wiley and Sons, Oxfort, United Kingdom

Tudjono, S., Han A.L., Gan, B.S., 2017. Revitalization of Cracked Flexural Members using Retrofitting and Synthetic Wrapping. *Procedia Engineering*, Volume 171, pp. 1123–1128

Tudjono, S., Han, A.L., Hidayat, A., Purwanto, 2017. Experimental Study on the Concrete Surface Preparation Influence to the Tensile and Shear Bond Strength of Synthetic Wraps. *Procedia Engineering*, Volume 171, pp. 1116–1122

Tudjono, S., Han, A.L., Hidayat, B.A., 2015. An Experimental Study to the Influence of Fiber Reinforced Polymer (FRP) Confinement on Beams Subjected to Bending and Shear. *Procedia Engineering*, Volume 125, pp. 1070–1075